Searching for Colorons at the Large Hadron Collider

Joshua Sayre[a][*], Duane A. Dicus[b][†], Chung Kao[a][‡], S. Nandi[c][§]

[a]*Homer L. Dodge Department of Physics and Astronomy*

and Oklahoma Center for High Energy Physics,

University of Oklahoma, Norman, OK 73019, USA

[b]*Center for Particles and Fields and Texas Cosmology Center,*

University of Texas, Austin, TX 78712, USA

[c]*Department of Physics and Oklahoma Center for High Energy Physics,*

Oklahoma State University, Stillwater, OK 74078, USA

Abstract

We investigate the prospects for the discovery of massive color-octet vector bosons at the CERN Large Hadron Collider with $\sqrt{s} = 14$ TeV. A phenomenological Lagrangian is adopted to evaluate the cross section of a pair of colored vector bosons (colorons, $\tilde{\rho}$) decaying into four colored scalar resonances (hyper-pions, $\tilde{\pi}$), which then decay into eight gluons. We include the dominant physics background from the production of $8g, 7g1q, 6g2q$, and $5g3q$, and determine the masses of $\tilde{\pi}$ and $\tilde{\rho}$ where discovery is possible. For example, we find that a 5σ signal can be established for $M_{\tilde{\pi}} \lesssim 495$ GeV ($M_{\tilde{\rho}} \lesssim 1650$ GeV). More generally we give the reach of this process for a selection of possible cuts and integrated luminosities.

PACS numbers: PACS numbers: 12.60.Rc, 13.85.Ni, 14.40.Rt, 14.70Pw

[*] Email address: sayre@physics.ou.edu
[†] Email address: dicus@physics.utexas.edu
[‡] Email address: kao@physics.ou.edu
[§] Email address: s.nandi@okstate.edu

I. INTRODUCTION

With the LHC beginning to accumulate data, we look forward to a new era of high-energy physics where we explore multi-TeV energy scales. In addition to the search for the Higgs boson to complete the Standard Model, many new physics scenarios have been considered as potential discoveries. Often, the discovery potential provided by the LHC's unprecedented collision energies is somewhat mitigated by the prevalence of jets from Standard Model processes. New physics which proceeds through weak interactions, such as Higgs production, must be carefully separated from large, strong-force produced backgrounds via judicious selection cuts.

It is also possible that new physics will manifest itself through the strong force. If new strongly interacting colored particles exist at TeV scales, they will be discovered through decays into jets. One generic possibility is a massive vector boson in the color-octet representation. Such a particle has been dubbed a coloron and several theories of physics beyond the Standard Model give rise to colorons. These include Kaluza-Klein excitations of the gluon in extra-dimensional models [1, 2], new states in top-color assisted technicolor [3], as well as models where the standard color group is a remnant of broken $SU(3) \times SU(3)$ [4]. In Ref. [5], Kilic, Okui, and Sundrum showed how colorons, as well as a scalar octet, can emerge as the low energy states of an effective theory arising from a simple model of new, strongly interacting fermions. In this paper we follow their analysis, as well as the subsequent treatment found in Ref. [6].

Briefly, we suppose that there exists a new, strongly coupled force, termed hypercolor, which becomes confining at higher energies than the QCD strong force. Fermions which carry hypercolor will form bound states which are hypercolor singlets but which may carry standard model charges. In particular, if these "hyperquarks" are also triplets of QCD then the lightest bound states will be color octets. Analogously to the breaking of chiral symmetry in the standard model, this model will produce relatively light hyper-pions as pseudo-Goldstone bosons, as well as colorons as bound states in the color octet representation.

This work assumes that the LHC will achieve its design center of mass energy of 14 TeV and accumulate data at that energy, and with high luminosity, over several years. In a separate paper, we have analyzed this coloron model for an energy of 7 TeV with an assumed

1 fb^{-1} or 5 fb^{-1} of total integrated luminosity [8]. We found that there is a chance of early detection from this early data set for hyper-pions up to a mass of 250 GeV.

In Section II we give some details of the explicit model we use. The colorons and octet scalars have an interesting phenomenology which we describe in Sec. III. In particular, we give some results for resonant $\tilde{\rho}$ production branching to two $\tilde{\pi}$ which decay into four jets. However, we argue that a more promising channel for coloron detection is coloron pair production followed by decay to four $\tilde{\pi}$ and then to eight jets. We show the results for this signal in Sec. IV and for the eight jet background in Sec. V. In Sec. VI we combine the signal and background to find a range of values of $M_{\tilde{\rho}}$ ($M_{\tilde{\pi}}$) where the $\tilde{\rho}$ could be discovered. In Sec. VII we summarize and conclude.

II. A MODEL WITH COLORED VECTOR BOSONS AND SCALARS

As in Ref. [5], we assume there is a new $SU(N)$ gauge group, hypercolor, acting on a new set of fermions which also carry Standard Model color charges. We expect this new force to become confining at a scale Λ_{HC}, resulting in a set of exotic mesons. Here one can consider an analogy with the breakdown of chiral symmetry in the Standard Model. If we neglect quark masses for the light quarks, there is a global $SU(3)_L \times SU(3)_R \times U(1)_L \times U(1)_R$ symmetry among the up, the down, and the strange quarks. Strong QCD interactions generate a quark-antiquark vacuum condensate which spontaneously breaks this symmetry down to $SU(3) \times U(1)$. In this simple picture one would expect 9 Goldstone bosons from the 9 broken currents, arranged in a flavor octet and a singlet. Realistically, the unequal quark masses and electric charges make these symmetries only approximate, especially when considering the relatively heavy strange quark. Rather than massless particles, we have pseudo-Goldstone bosons with the familiar pions as a light isospin triplet and somewhat heavier kaons and etas filling out the nonet. This division within the nonet is due primarily to the strange quark. The isospin singlet is also heavier than the pions due to a non-vanishing anomaly in the isosinglet-gluon-gluon diagram, meaning this current is not conserved in QCD. These scalars also have heavier, spin-1 counterparts in the ρ, K^*, ω, and ϕ mesons.

For the hypercolor model a similar analysis applies. Massless hyperquarks would have a global left-right flavor symmetry which is spontaneously broken by a hypercolor-driven condensate. In the Standard Model case there is an approximate remaining flavor symmetry

3

due to the lightness of the up, down, and strange quarks. In the present example, however, this role is filled by the SM gauged $SU(3)$ color symmetry which remains exact. Hence the left-right flavor breaking should preserve a color nonet of pseudo-Goldstone bosons, assuming that any mass terms for the hyperquarks are suitably below the scale of symmetry breaking. This nonet can be decomposed as a massive color octet and a singlet. Similarly to the isospin singlet mentioned above, the color singlet will have a non-vanishing anomaly with two hyper-gluons and we do not expect it to be as light as the octet. The lightest new states in the effective theory are thus a color octet of scalars, which are designated "hyper-pions" ($\tilde{\pi}$) in reference to their standard model analogues. These states should have a set of spin-1 excitations which fill out a massive color octet of vector bosons. These "hyper-rhos" ($\tilde{\rho}$) are called colorons in the naming convention we follow.

Based on this model of chiral symmetry breaking, the authors of Ref. [5] derive the following effective Lagrangian:

$$
\begin{aligned}
\mathcal{L}_{\text{eff}} = {} & -\frac{1}{4}G^a_{\mu\nu}G^{a\mu\nu} + \bar{q}i\slashed{D}q - g_3\epsilon\tilde{\rho}^a_\mu\bar{q}\gamma^\mu T^a q \\
& +\frac{1}{2}(D_\mu\tilde{\pi})^a(D^\mu\tilde{\pi})^a - M_{\tilde{\pi}}{}^2\tilde{\pi}^a\tilde{\pi}^a - \frac{1}{4}\tilde{\rho}^a_{\mu\nu}\tilde{\rho}^{a\mu\nu} + \frac{M_{\tilde{\rho}}^2}{2}\tilde{\rho}^a_\mu\tilde{\rho}^{a\mu} \\
& -ig_{\tilde{\rho}\tilde{\pi}\tilde{\pi}}f^{abc}\tilde{\rho}^{a\mu}(\tilde{\pi}^b D_\mu\tilde{\pi}^c) - \frac{3g_3{}^2\epsilon^{\mu\nu\rho\sigma}}{16\pi^2 f_{\tilde{\pi}}}\text{Tr}[\tilde{\pi}G_{\mu\nu}G_{\rho\sigma}] \\
& +i\chi g_3 \text{Tr}[G_{\mu\nu}[\tilde{\rho}^\mu,\tilde{\rho}^\nu]] + \xi\frac{2i\alpha_3\sqrt{N_{\text{HC}}}}{M_{\tilde{\rho}}^2}\text{Tr}[\tilde{\rho}^\mu_\nu[G^\nu_\sigma, G^{\sigma\mu}]].
\end{aligned} \tag{1}
$$

For simplicity, we assume only one flavor of hyper-quark, Q so that we have only one pseudo-Goldstone boson $\tilde{\pi}$ and one $Q\bar{Q}$ bound state, $\tilde{\rho}$. In the above equation $G_{\mu\nu}$ and q are Standard Model gluon and quark fields, while a is a color index. $SU(N_{\text{HC}})$ is the the symmetry group of the hypercolor gauge interaction and we will take N_{HC} to be 3 for simplicity. Based on this assumption, Kilic et al. have derived most of the parameters in terms of a single variable, $M_{\tilde{\rho}}$. They find $\varepsilon \simeq 0.2$, $g_{\tilde{\rho}\tilde{\pi}\tilde{\pi}} \simeq 6$, $M_{\tilde{\pi}} \simeq 0.3M_{\tilde{\rho}}$, and $f_{\tilde{\pi}} \simeq f_\pi\frac{M_{\tilde{\rho}}}{m_\rho}$ where $f_\pi = 92$ MeV, the standard pion decay constant, and m_ρ is the mass of the ordinary ρ meson [6, 7].

The first line of the Lagrangian contains Standard Model QCD, plus the potential for quarks to couple to the $\tilde{\rho}$. The second line contains kinematic and mass terms for the $\tilde{\pi}$ and $\tilde{\rho}$ with D_μ representing the SM covariant derivative. The third line contains the couplings of the $\tilde{\rho}$ to two $\tilde{\pi}$'s and the coupling of $\tilde{\pi}$ to two gluons which provide the primary decay routes of interest to us because of the large coupling strength $g_{\tilde{\rho}\tilde{\pi}\tilde{\pi}}$ and the relatively suppressed pion-

gluon-gluon coupling. The last two terms of equation (1) give additional gluon couplings to the $\tilde{\rho}$. They contain the parameters χ and ξ, which cannot be extrapolated from the Standard Model analogy as they would vanish in the Abelian case. Other models, such as the topcolor model require $\chi = 1$ and $\xi = 0$. Further these are the only values for which any model is unitary. After we compare the cross section $pp \to \tilde{\pi}\tilde{\pi} + X$ for a few values of ξ and the cross section $pp \to \tilde{\rho}\tilde{\rho} + X$ for a few values of χ we will set ξ and χ to the unitary values for the rest of the paper (Sec. IV A and beyond).

III. GENERAL PHENOMENOLOGY

Based on the model outlined above, the hyper-pion couples to gluons via an anomalous term which we may think of as a triangular loop involving hyper-quarks. This is similar to the decay of the Standard Model π^0 into two photons. The hyper-pion decay width is given by

$$\Gamma_{\tilde{\pi}\to gg} = \frac{15\alpha_s^2 M_{\tilde{\pi}}^3}{256\pi^3 f_{\tilde{\pi}}^2}. \tag{2}$$

The $\tilde{\pi}$s will thus appear as a decay into two jets and can potentially be produced singly via gluon fusion. The $\tilde{\rho}$, on the other hand, couples to quarks through coloron-gluon mixing, as well as to gluons for non-zero values of ξ. However, its dominant decay mode is into two $\tilde{\pi}$s due to the large coupling $g_{\tilde{\rho}\tilde{\pi}\tilde{\pi}}$. Thus for a large range of parameters the observable coloron decay is four jets arising from two hyper-pion resonances. For $\xi = 0$ the $\tilde{\rho}$ decay width, as a function of $M_{\tilde{\rho}}$, is

$$\Gamma_{\tilde{\rho}} \simeq 0.19 M_{\tilde{\rho}}, \tag{3}$$

with a branching fraction to $\tilde{\pi}$s of $B(\tilde{\rho} \to \tilde{\pi}\tilde{\pi}) \simeq 95\%$. One can see that the decay width for the $\tilde{\rho}$ relative to its mass is quite broad, while that for the $\tilde{\pi}$ is narrow.

The dijet decay modes of both the scalar and the vector octets provide possible constraints on the model because of the dijet resonance exclusion bounds from the Tevatron Run-II data [9, 11]. However, for the coloron, the branching ratio to dijets is small (less than 5 percent), suppressing the signal below existing bounds. This would not be true without the strongly coupled pion decay mode, as can be seen in Fig. 1. In this figure the solid black line shows the bound for dijet decays of a coloron-like particle at the CDF detector [9]. The dashed (red) curve represents the total cross section for $pp \to \tilde{\rho} \to jj + X$ in the absence of
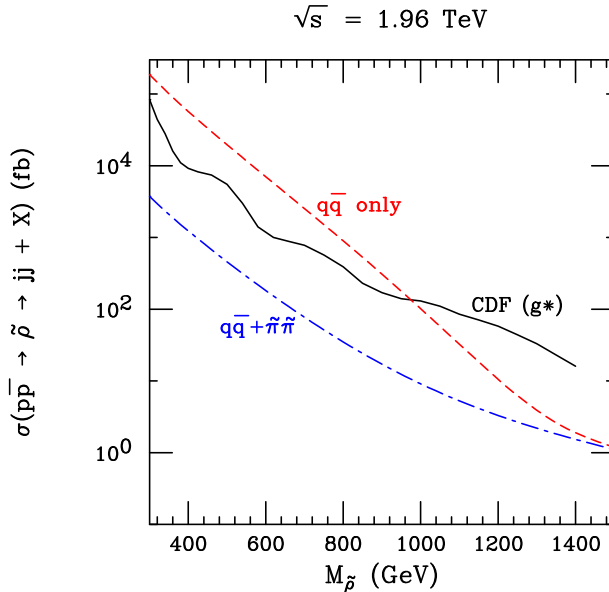
FIG. 1: CDF exclusion limits (black solid line) for dijet-decaying color octets, compared to predicted $pp \to \tilde{\rho} \to jj + X$ cross sections computed with $\tilde{\pi}$ decays (blue dot-dashed line) and without $\tilde{\pi}$ decays (red dashed line) for $\sqrt{s} = 1.96$ TeV.

the pion decay mode. The dot-dash (blue) line indicates the total dijet cross section with this mode taken into account. One can see that without the large pion contributions to the $\tilde{\rho}$ width, colorons would be ruled out below about 1 TeV. As shown in Fig. 2 the LHC early searches for exotic dijet resonances [10] are not yet competitive with the CDF bound [9]. Hence, it will be difficult to observe a signal for the coloron via this dijet mode.

A natural channel to search for the coloron is the resonant $\tilde{\rho}$ production branching to two $\tilde{\pi}$'s which decay into four jets. This mode has been studied for the Tevatron in Ref. [5] and for the LHC in Ref. [6]. For comparison we present our results for the production cross section $pp \to \tilde{\pi}\tilde{\pi} + X$ as a function of $M_{\tilde{\pi}}$ in Fig. 3. In addition, Fig. 4 shows the possible enhancement of the signal with a non-zero value for ξ. We note that our results appear to be smaller than those shown in the equivalent figure of Kilic et al. by approximately a factor of two.

However, as pointed out in Ref. [6], if our goal is to distinguish the primary coloron resonance, this mode presents some difficulties, particularly at the LHC. Although the $\tilde{\pi}$ resonances should be clear for accessible mass ranges, this may not be the case for the coloron. While the hyper-pion decay width is quite small compared to its mass, leading to a
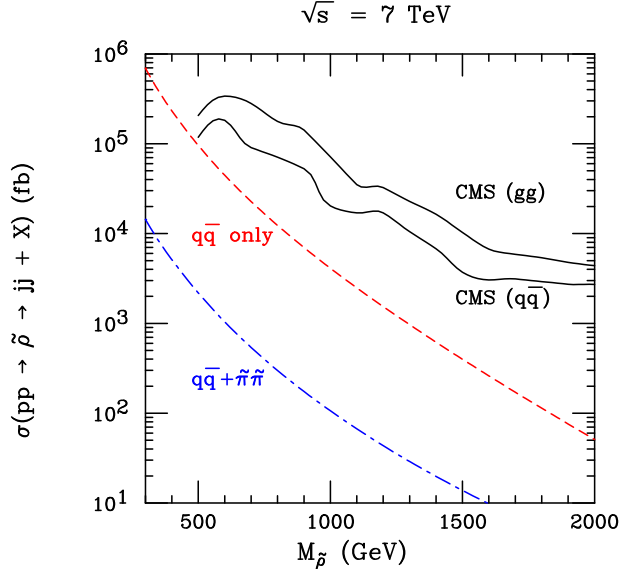
FIG. 2: CMS exclusion limits (black solid line) for dijet-decaying color octets, compared to predicted $pp \to \tilde{\rho} \to jj + X$ cross sections computed with $\tilde{\pi}$ decays (blue dot-dashed line) and without $\tilde{\pi}$ decays (red dashed line) for $\sqrt{s} = 7$ TeV.

sharp peak in the pair invariant 2-jet mass distribution, the $\tilde{\rho}$ has a large width ($\sim 0.2 M_{\tilde{\rho}}$) leading to a broad peak. Moreover, there are important alternate modes of hyper-pion pair production in this model, which do not involve the coloron, as shown in Fig. 5.

The first graph of Fig. 5, A, is negligible owing to the smallness of the $g - g - \tilde{\pi}$ vertex but the others comprise a significant part of the two-$\tilde{\pi}$ signal. These contributions derive from two initial gluons, thus they are especially important at the LHC.

The importance of non-resonant diagrams can be seen in Fig. 6. This plot was produced for $M_{\tilde{\rho}} = 750$ GeV ($M_{\tilde{\pi}} = 225$ GeV) for $\sqrt{s} = 14$ TeV. Only minimal cuts were applied; all jets were required to have $p_T > 15$ GeV and $|\eta| < 2.5$ and all pairs of jets were required to be separated by $\Delta R > 0.5$. We consider the signal $pp \to \tilde{\rho} \to \tilde{\pi}\tilde{\pi} \to 4g + X$ and apply a Gaussian smearing routine to outgoing momenta. There are 3 ways of pairing up the 4 final jets and we require that at least one such pairing results in two pair masses within 50 GeV of each other. The solid (blue) curve represents the invariant mass of a pair of jets. This curve shows the average mass obtained thereby and one can clearly see the hyper-pion peak. (If more than one arrangement allows two nearby pair masses, we average over these as well.) The signal reconstruction away from the main peak can be reduced by narrowing the 50 GeV window.
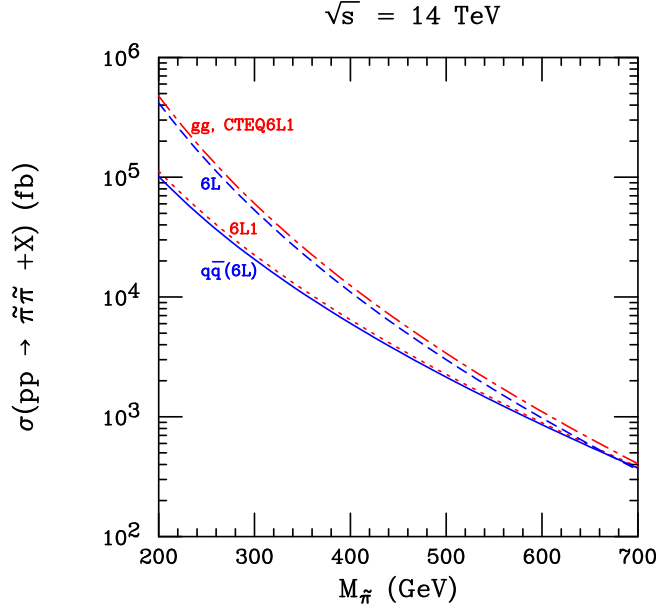
FIG. 3: The cross section of $pp \to \tilde{\pi}\tilde{\pi} + X$ from gg and $q\bar{q}$ as a function of $M_{\tilde{\pi}}$. We compare cross sections for two sets of parton distribution functions, CTEQ6L1 and CTEQ6L. [14]

The dashed (red) curve shows the 4−jet invariant mass constructed from the sum of the final state momenta. The peak is not located at the 750 GeV region; in fact the $\tilde{\rho}$ mass appears as only a broad local maximum. It is difficult to improve the coloron detection in this channel without foreknowledge of the $\tilde{\pi}$-$\tilde{\rho}$ mass relation.

For this reason we focus in this paper on an alternate detection channel. We investigate the possibility of pair-produced colorons at the LHC, $pp \to \tilde{\rho}\tilde{\rho} \to 4\tilde{\pi} \to 8g + X$. Pair production of $\tilde{\rho}$'s receives contributions from both gg and $q\bar{q}$ initial states. More importantly, the presence of two identical massive resonances allows us a better chance of distinguishing them by correlating 4-jet invariant masses. Fig. 7 was calculated from the four hyper-pion signal at the LHC. Similarly to the hyper-pion signal represented in Fig. 6, we simulate events and reconstruct an average mass for two pairs of hyper-pions with invariant masses within 100 GeV of each other. The peak, shown with a solid (blue) or a dashed (red) curve, is broad but it is clearly located at the chosen $\tilde{\rho}$ mass of 750 GeV or 1500 GeV, even though we have not made any assumptions to influence that value in our reconstruction. Despite the fact that the calculated signal, $pp \to 4\tilde{\pi} + X$ includes hundreds of graphs without any intermediate $\tilde{\rho}$s, only those which do have intermediate $\tilde{\rho}$s are likely to contribute significantly to the correlated signal. The peak at the correct mass should improve with a narrower window,
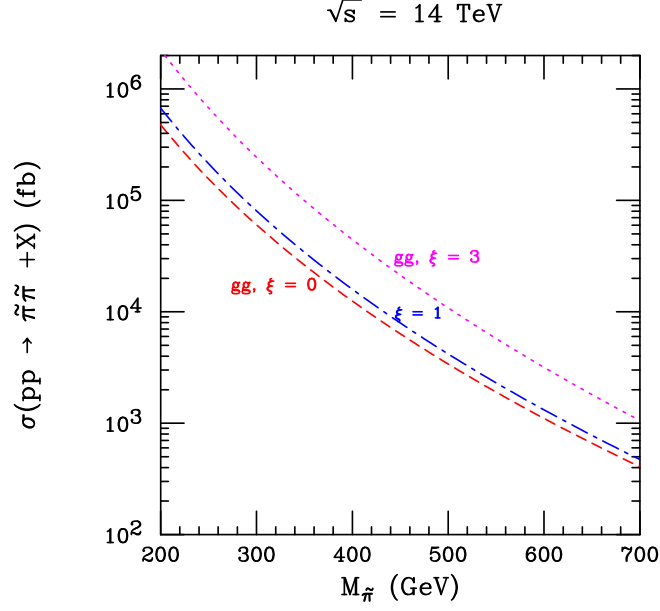
8

FIG. 4: The cross section of $pp \to \tilde{\pi}\tilde{\pi} + X$ from gluon initial states, as a function of $M_{\tilde{\pi}}$, for $\xi = 0, 1$, and 3.
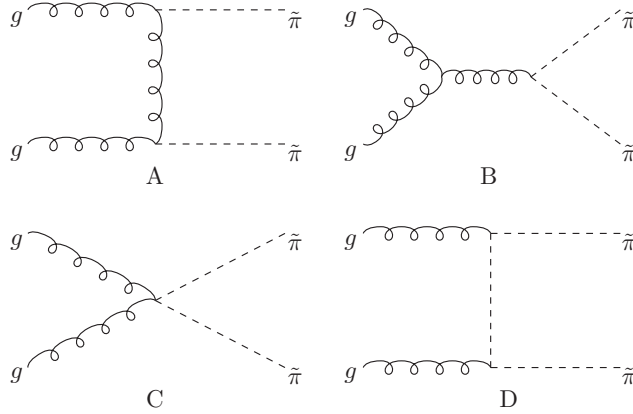

FIG. 5: Feynman diagrams of $gg \to \tilde{\pi}\tilde{\pi}$.

but we must be careful not to restrict it too much. The inherently broad width of the $\tilde{\rho}$, compounded by the resolution limitations of a real detector caution against killing our signal with over-fine mass searches.
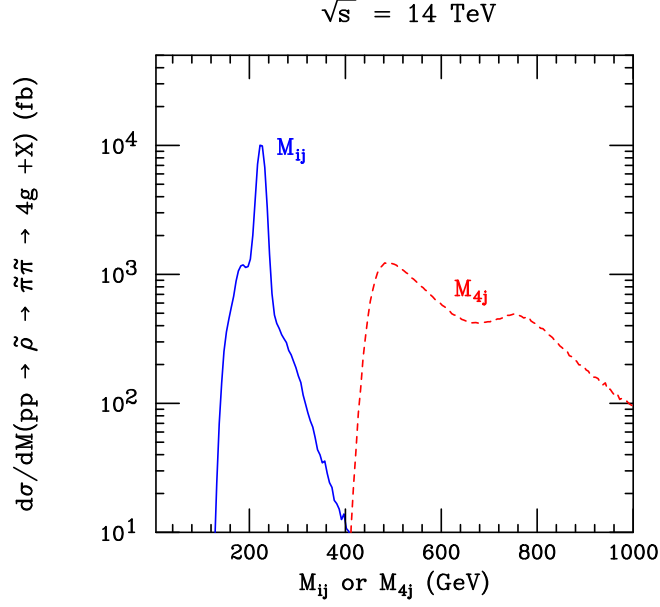
FIG. 6: Invariant mass distribution of two jets (M_{jj}) or four jets (M_{4j}) from $pp \to \tilde{\rho} \to \tilde{\pi}\tilde{\pi} \to 4g + X$.
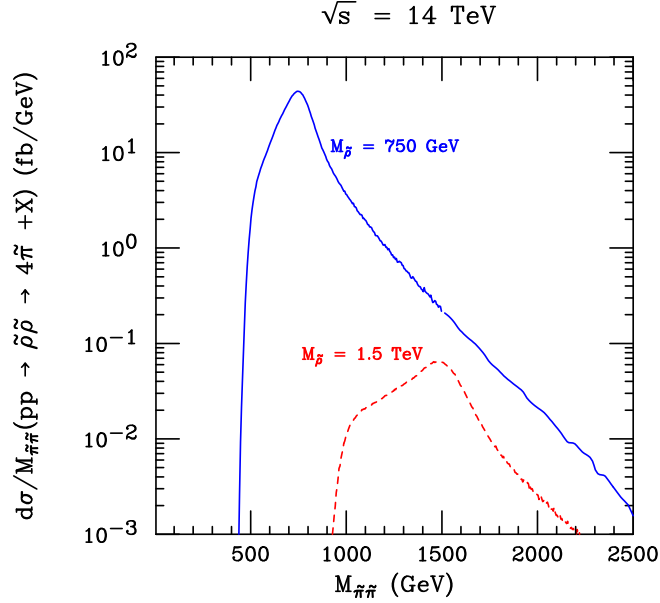

FIG. 7: Invariant mass distribution of two $\tilde{\pi}$'s for $pp \to 4\tilde{\pi} + X$ with $\sqrt{s} = 14$ TeV.

IV. SIGNAL SIMULATION

Our chosen signal is $pp \to \tilde{\rho}\tilde{\rho} \to 4\tilde{\pi} \to 8g + X$. In order to run Monte-Carlo simulations of events we make use of MadGraph II [15, 16] to generate the squared matrix elements. We

have built the coloron model into the MadGraph/MadEvent4 code using the available "user model" framework. However, to implement the full model we have made some modifications to the underlying code for generating color factors and we have added some additional routines to the HELAS library [17] used by MadGraph. This is necessitated by the non-Standard-Model vertices which facilitate some of our interactions. The $g - \tilde{\rho} - \tilde{\rho}$ vertex, for example, is similar to the Standard Model 3-gluon interaction, but contains a χ dependence for the terms involving the gluon momentum.

The authors of refs [5] and [6] implemented the model in the AMEGIC matrix element generator which is used by the SHERPA event generator. We have chosen to build the model into MadGraph so as to have an independent calculation of the relevant cross sections. We calculate our backgrounds with SHERPA.

In the case of the $pp \to 8g + X$ decay chain, we had to make some modifications to handle the very large terms which arise in the color factors. The complete $pp \to 8g + X$ matrix element with all permutations of virtual particles is beyond the powers of MadGraph4 to generate due to the large number of graphs. Fortunately, the $\tilde{\pi}$ has a very small width relative to its mass, making it an excellent candidate for the Narrow Width Approximation (NWA). This small width means that interference terms between different arrangements of virtual hyper-pions are small compared to the resonant contributions. Thus we are able to generate the matrix element $pp \to (\tilde{\rho} \to (\tilde{\pi} \to gg)(\tilde{\pi} \to gg))(\tilde{\rho} \to (\tilde{\pi} \to gg)(\tilde{\pi} \to gg)) + X$ including the $\tilde{\pi}$ width. This should be an excellent approximation to the complete calculation, and checking the $pp \to 2\tilde{\rho} \to 4\tilde{\pi} + X$ matrix element with on-shell hyper-pion decays we do find very good agreement. Thus the NWA for the $\tilde{\pi}$s is valid and we make use of it for our signal generation. The width of the $\tilde{\rho}$ on the other hand makes the NWA unsuitable for that particle and we keep its width and interference terms throughout.

To further check our MadGraph results we have done an independent analytic calculation of the $gg \to 2\tilde{\rho} \to 4\tilde{\pi}$ matrix element, including the χ and width dependence. Tested with realistic momenta, we have near-perfect concordance of numerical results from the two computations.

For completeness we present here our analytic formula for the square of the matrix element $gg \to \tilde{\rho}\tilde{\rho}$, summed over polarizations and colors, as a function of χ. We neglect the coloron

width as it would make for a substantially longer expression.

$$
\sum_{\text{pol}} |T|^2 = \frac{Y^2(1-z^2)^2}{(1-\beta^2 z^2)^2} \frac{E^4}{M_{\tilde{\rho}}^4} \left[12 - 12Y + (5+z^2)Y^2 \right]
$$

$$
+ \frac{Y^2(1-z^2)}{(1-\beta^2 z^2)^2} \frac{E^2}{M_{\tilde{\rho}}^2} \left[16(1+3z^2) - 2(11+18z^2)Y + (5+9z^2+3z^4)Y^2 \right]
$$

$$
+ \frac{1}{(1-\beta^2 z^2)^2} \left[8 \left(16 + 3\frac{M_{\tilde{\rho}}^4}{E^4} \right) - 256Y + (160 + 16z^2 + 36z^4)Y^2 \right.
$$

$$
\left. - (32 + 22z^2 + 24z^4)Y^3 + (2 + 5z^2 + 4z^4 + 2z^6)Y^4 \right]
$$

$$
+ \frac{1}{1-\beta^2 z^2} \left[-6 \left(16 + 4\frac{M_{\tilde{\rho}}^2}{E^2} + \frac{M_{\tilde{\rho}}^4}{E^4} \right) + 140Y - (58 + 24z^2)Y^2 \right.
$$

$$
\left. + 3(1 + 4z^2)Y^3 - z^4 Y^4 \right]
$$

$$
+ 28 + 6\frac{M_{\tilde{\rho}}^2}{E^2} - 3(1 - \beta^2 z^2) - 16Y + 4Y^2 , \tag{4}
$$

where E is the gluon c.m. energy, z is the cosine of the scattering angle, $\beta^2 = 1 - M_{\tilde{\rho}}^2/E^2$, and $Y = 1 - \chi$.

It is interesting to compare this to another calculation of coloron pair production in a somewhat different model, given in Ref. [4]. In that model, colorons arise from the spontaneous breaking of an $SU(3)_I \times SU(3)_{II}$ gauge symmetry to the familiar $SU(3)_{color}$. (In the topcolor model, the $SU(3)_I$ couples to the first two families of the SM fermions, while the $SU(3)_{II}$ couples to the 3rd family.) This results in a set of massive partners to the SM gluons through a Higgs mechanism, and these colorons are similar to the ones we discuss. However, they do not have the χ dependence shown above and we have checked that our formula is equivalent for the case $\chi = 1$. Recall that in the model we consider, the colorons are not the product of a broken gauge symmetry, but are composite particles ($Q\bar{Q}$) of the hyper-quarks. In the limit where $\chi \to 1$ the $\tilde{\rho}$s couple to gluons in exactly the same fashion as other gluons, so perhaps it is not too surprising that they then mimic the "hyper-gluons" of the model of Ref. [4].

Only for $\chi = 1$ is the theory given in Eq. (1) explicitly unitary for $gg \to \tilde{\rho}\tilde{\rho}$. This can be seen in Eq. (4) above where the first lines grow with energy unless $Y = 0$. In general the coloron model we consider is only an effective theory which results from integrating out heavy, strongly-interacting hyper-quarks. The Lagrangian includes non-renormalizable terms and does not include any explicit hyper-color gauge fields, nor does it explain the

12

origin of hyper-quark masses. Thus as a theory of massive vector bosons we do not expect it to preserve unitarity to all energies. In the $\chi = 1$ case, however, the $\tilde{\rho}$s have gluon couplings equivalent to the colorons of spontaneously broken $SU(3)_I \times SU(3)_{II}$. In that model we think of the longitudinal components of the massive bosons as coming from 'eaten' Higgs fields, and in the high-energy limit unitarity is restored by the Goldstone Boson Equivalence theorem and the underlying gauge invariance, just as in the case of W^+W^- scattering.

In Fig. 8 we show the total two-$\tilde{\rho}$ production cross section as a function of the coloron mass. We include the prediction for $\chi = 0$, 1, and 3 to demonstrate the effect of this parameter. This figure may be compared to the results shown in Ref. [6]. Our estimates are broadly consistent. However, for some parameters their predicted cross section appears to be as much as twice our result. The discrepancy is more pronounced at high values of $M_{\tilde{\rho}}$ and for non-unitary values of χ. Henceforth we will use χ equal to one.
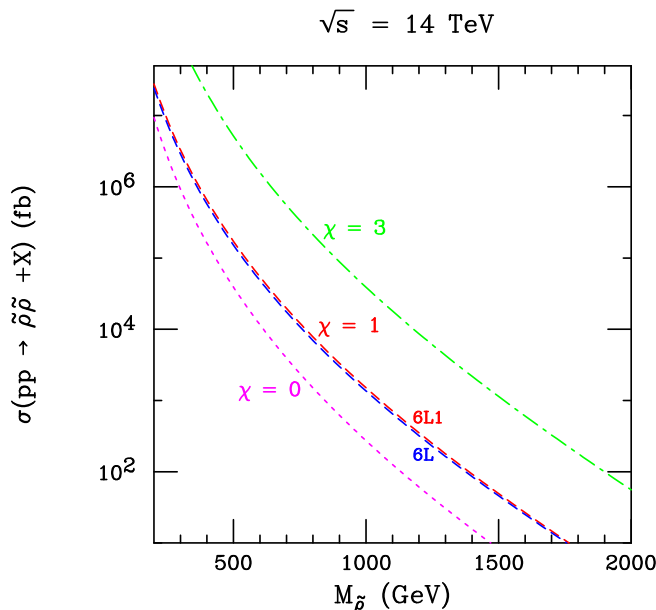

FIG. 8: The cross section of $pp \to \tilde{\rho}\tilde{\rho} + X$, as a function of $M_{\tilde{\rho}}$, for $\chi = 1, 0$, and 3.

The parameter ξ, which scales the $g - g - \tilde{\rho}$ vertex, can enhance the signal if it has a non-zero value. This vertex derives from a non-renormalizable term in the effective Lagrangian, which is the lowest order term allowing a direct gluon-$\tilde{\rho}$ coupling. Its effect on the two $\tilde{\rho}$ signal is shown in Fig. 9 for $\xi = 1$ (dotted, green), $\xi = 3$ (dot-dash, black) and $\xi = 10$ (dashed, blue) compared to $\xi = 0$ (solid, red). Order one values of ξ would significantly enhance the signal in the lower mass range. The effect is insensitive to the sign of ξ. (The

four-jet, single-$\tilde{\rho}$ channel would also be enhanced, with potentially better resolution of the $\tilde{\rho}$ resonance since ξ does not contribute to the non-resonant pion-pair graphs.)
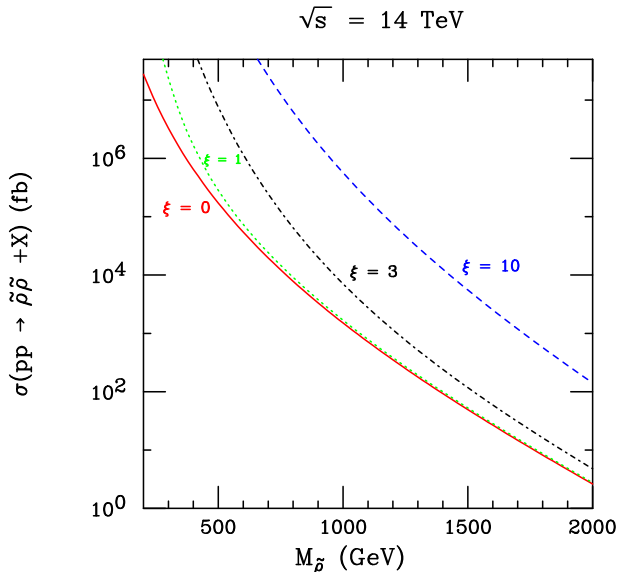

FIG. 9: The cross section of $pp \to \tilde{\rho}\tilde{\rho} + X$, as a function of $M_{\tilde{\rho}}$, for $\xi = 0, 1, 3$, and 10 at the LHC with $\sqrt{s} = 14$ TeV.

On the other hand, increasing ξ also affects the dijet signal and potentially runs afoul of the Tevatron exclusion bound, as shown in Fig. 10. For $\xi = 1$ (dash, red) the dijet prediction is virtually the same as for $\xi = 0$ (solid, blue). However if ξ is allowed to be as large as 10 (dotted, green), then the current bounds require $M_{\tilde{\rho}}$ to be greater than a few-hundred GeV. For the remainder of the paper we will set $\xi = 0$, the most conservative choice.

A. Signal Selection

We proceed to generate signal samples using our MadGraph-generated matrix elements and decaying the hyper-pions via the NWA. These are convoluted with the CTEQ6L1 parton distribution functions. For the signal we have followed the prescription that we use the mass of the pair produced particle as the factorization and renormalization scale, i.e. $\mu_F = \mu_R = M_{\tilde{\rho}}$. We take the K-factor to be one. We apply a Gaussian smearing routine to the outgoing momenta based on ATLAS specifications [18]
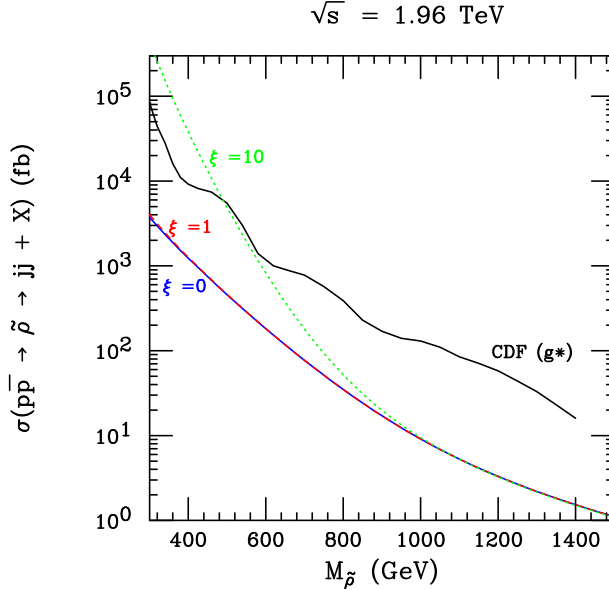
FIG. 10: The cross section of $pp \to \tilde{\rho} \to jj + X$ for $\xi = 0, 1$, and 10, compared to exclusion bounds at the Tevatron CDF detector.

$$\frac{\Delta E}{E} = \frac{0.60}{\sqrt{E(\text{GeV})}} \oplus 0.03 \ . \tag{5}$$

In all cases we require that the final gluons are within $-2.5 < \eta < 2.5$ and separated from one another by $\Delta R > 0.5$, so we assume they are reconstructed as eight jets. These jets should have a high p_T distribution in general due to boosts from the heavy $\tilde{\rho}$ and $\tilde{\pi}$ decays. Ordered by p_T, the outgoing gluon p_T profiles present a succession of peaks, as shown in Fig. 11. We find that the leading p_T gluon typically peaks around $\frac{M_{\tilde{\rho}}}{2} \simeq 1.5 M_{\tilde{\pi}}$. Particularly for high coloron masses, high p_T cuts on the leading jets provide strong discrimination against the background.

Aside from transverse momentum requirements, our primary tool for reducing background is selection for invariant masses. We have pursued two different cut algorithms for this purpose.

B. Relative Mass Windows

For *relative* mass cuts we require that there is an arrangement of the 8 gluons into 4 pairs such that the largest and smallest invariant masses of these pairs are within a given window
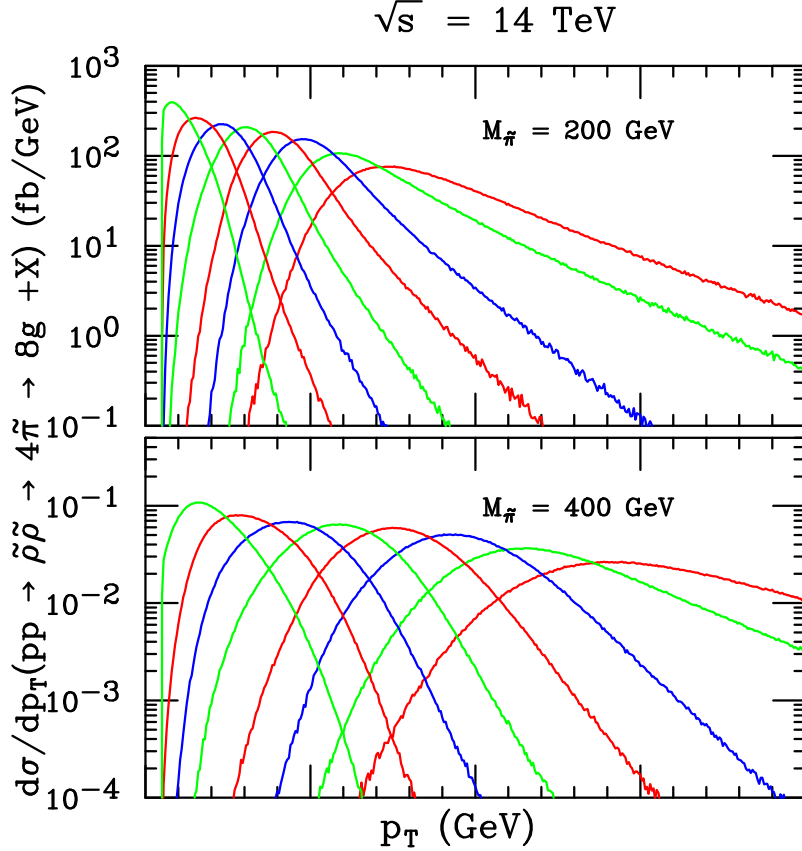
FIG. 11: Transverse momentum (p_T) distributions of the eight signal gluons for $M_{\tilde{\pi}} = 200$ GeV (top) and $M_{\tilde{\pi}} = 400$ GeV (bottom).

of one another (ΔM_{ij}). We then require that these candidate hyper-pions can be arranged into pairs such that the two pion-pair (4-gluon) invariant masses are within a window ΔM_{4j}. A successful arrangement of the gluons into candidate hyper-pions and colorons must satisfy both mass window requirements simultaneously. For example, a set of gluons $1, \ldots, 8$ which passes the pion cut with the arrangement $(12)(34)(56)(78)$ can pass the rho cut with 4-masses such as $(1234)(5678)$ but not with $(1235)(4678)$.

Fig. 12 shows a plot of the signal for $M_{\tilde{\pi}} = 225$ GeV and $M_{\tilde{\rho}} = 750$ GeV based on relative window mass cuts with $\Delta M_{ij} = 50$ GeV and $\Delta M_{4j} = 100$ GeV. Minimal momentum cuts of $p_T > 15$ GeV are applied. The solid (blue) line shows the average of candidate hyper-pion masses which pass the cuts, and it is sharply peaked at the hyper-pion mass. The dashed (red) line shows the average candidate coloron mass which is peaked at the coloron mass as expected. The equivalent lines corresponding to physical masses $M_{\tilde{\pi}} = 450$ GeV and

$M_{\tilde{\rho}} = 1.5$ TeV are shown with solid (blue) and dashed (red) curves respectively.
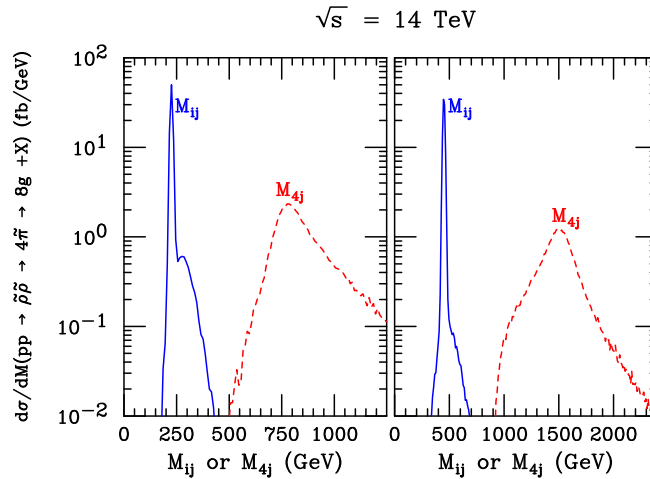

FIG. 12: Invariant mass distribution of two jets or four jets for $pp \to \tilde{\rho}\tilde{\rho} \to 4\tilde{\pi} \to 8g + X$.

C. Fixed Mass Windows

For *fixed* mass cuts we require a suitable arrangement of gluons into candidate $\tilde{\pi}$s and $\tilde{\rho}$s as above. But rather than requiring that the reconstructed masses are each within some window of one another, we require that they all fall within a window around a set mass. That is, we require all four M_{ij}s to satisfy $|M_{ij} - M_{\tilde{\pi}}| < \Delta M_{ij}$ and the 4-gluon invariant masses corresponding to pairs of candidate hyper-pions to satisfy $|M_{4j} - M_{\tilde{\rho}}| < \Delta M_{4j}$ for a chosen value of $M_{\tilde{\pi}}$ or $M_{\tilde{\rho}}$.

The advantage of the relative mass scheme is that it requires no prior assumptions about the $\tilde{\pi}$ or $\tilde{\rho}$ masses. It is based only on correlations between the invariant masses within an experimental data set. On the other hand it is effectively sampling across all possible masses so it is not as efficient as we might like for eliminating backgrounds. The fixed mass scheme will perform better against background if the parameters $M_{\tilde{\pi}}$ and $M_{\tilde{\rho}}$ are chosen close to the actual physical masses of the particles. Probable values for these parameters can, for example, be read off a plot similar to Fig. 12 derived from a relative mass window analysis. Or we may imagine that the hyper-pion mass is established by sliding a fixed pair-invariant-mass window to find signal over background excesses in the 8-jet or 4-jet channels. One could then test choices of $M_{\tilde{\rho}}$ for a fixed value of $M_{\tilde{\pi}}$.

V. BACKGROUND SIMULATION

The background for our signal is 8 jets coming from Standard Model QCD processes. Obviously it is quite large and complex before p_T and invariant mass cuts. MadGraph/MadEvent4 cannot simulate more than 5 outgoing gluons with all terms included. Instead we rely on the SHERPA 1.2.2 [19] event generator. SHERPA makes use of the COMIX [20] matrix element calculator, which applies color-dressed Berends-Giele recursion relations [21]. For numerical calculations of high-multiplicity tree-level diagrams this seems to be the most efficient method currently available [22]. We again use CTEQ6L1 PDFs but with the renormalization and factorization scales set to $\sqrt{\langle p_T^2 \rangle}$, the root mean transverse momentum squared. We take the K factor to be one. Cuts are applied as described for the signal.

The dominant backgrounds we consider are QCD processes for $pp \rightarrow 8j+X$ from $gg \rightarrow 8g$, $gq \rightarrow 7g1q$, $gg, qq \rightarrow 6g2q$, and $gq \rightarrow 5g3q$, where q may be a quark or an antiquark. We expect these to account for the bulk of the background since diagrams with higher numbers of quarks have relatively suppressed color factors and fewer graphs. Of the backgrounds we compute, which process dominates depends on the cuts we choose and the mass of the hyper-mesons. This behaviour can be seen in Fig. 13.

At low masses where we generally consider lower p_T cuts, the $gg \rightarrow 8g$ (dash, red) channel tends to be largest, followed by $gq \rightarrow 7g1q$ (solid, green) and $gg \rightarrow 6g2q$ (dash-dot, magenta). As we move to higher masses and p_T requirements, valence quarks in the initial state become more important since they are favored when the kinematics require a large fraction of the incoming proton's momentum. Thus $gq \rightarrow 7g1q$ becomes the largest contribution for much of our range while $gg \rightarrow 8g$, $gq \rightarrow 5g3q$ (dash, blue), and $qq \rightarrow 6g2q$ (dash-dot, black) are subdominant with comparable values and $gg \rightarrow 6g2q$ becomes an increasingly small fraction of the total. For very high masses and cuts, $qq \rightarrow 6g2q$ becomes the largest background since it is the only one which can have two up or two down quarks in the initial state. We have found that the background $qq \rightarrow 8g$ is consistently smaller than the dominant processes by more than an order of magnitude and we neglect it in our results.

We also include the next two possibly significant backgrounds in the figure, $qq \rightarrow 4g4q$ (dot, black) and $gg \rightarrow 4g4q$ (solid, cyan). They remain well below the dominant channels for observable $M_{\tilde{\pi}}$ and we do not include them in the background estimates.
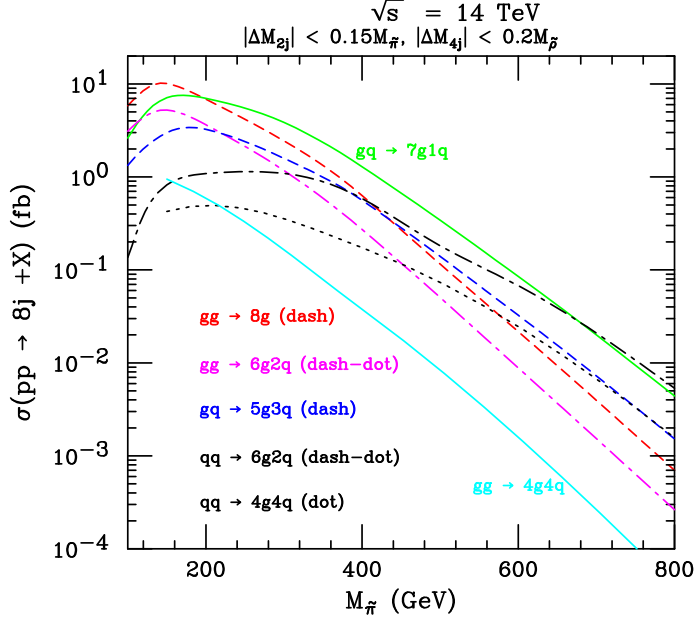
FIG. 13: Individual background channels for $pp \to 8j + X$, calculated with fixed mass window cuts and $p_T(j_1) > 1.5M_{\tilde{\pi}}$, $p_T(j_2) > 1.2M_{\tilde{\pi}}$, $p_T(j_3) > M_{\tilde{\pi}}$, $p_T(j_4) > 0.8M_{\tilde{\pi}}$, $p_T(j_5, j_6, j_7, j_8) > 50\,\mathrm{GeV}$.

VI. DISCOVERY POTENTIAL AT THE LHC

Our results for the signal and background at the LHC with $\sqrt{s} = 14$ TeV are presented in Fig. 14, 15 and 16. To estimate the discovery potential at the LHC we include curves that correspond to the minimal cross section of signal (σ_s) required by our discovery criterion described in the following. We define the signal to be observable if the lower limit on the signal plus background is larger than the corresponding upper limit on the background [23] with statistical fluctuations

$$L(\sigma_s + \sigma_b) - N\sqrt{L(\sigma_s + \sigma_b)} \geq L\sigma_b + N\sqrt{L\sigma_b} \tag{6}$$

or equivalently,

$$\sigma_s \geq \frac{N}{L}\left[N + 2\sqrt{L\sigma_b}\right]. \tag{7}$$

Here L is the integrated luminosity, σ_s is the cross section of the coloron signal, and σ_b is the background cross section. The parameter N specifies the level or probability of discovery. We take $N = 2.5$, which corresponds to a 5σ signal. For $\sigma_b \gg \sigma_s$, this requirement becomes similar to

$$N_{\mathrm{SS}} = \frac{N_s}{\sqrt{N_b}} = \frac{L\sigma_s}{\sqrt{L\sigma_b}} \geq 5,$$

19

where N_s is the signal number of events, N_b is the background number of events, and $N_{\text{SS}} =$ the statistical significance, which is commonly used in the literature. If the background has fewer than 25 events for a given luminosity, we employ the Poisson distribution and require that the Poisson probability for the SM background to fluctuate to this level is less than 2.85×10^{-7}.
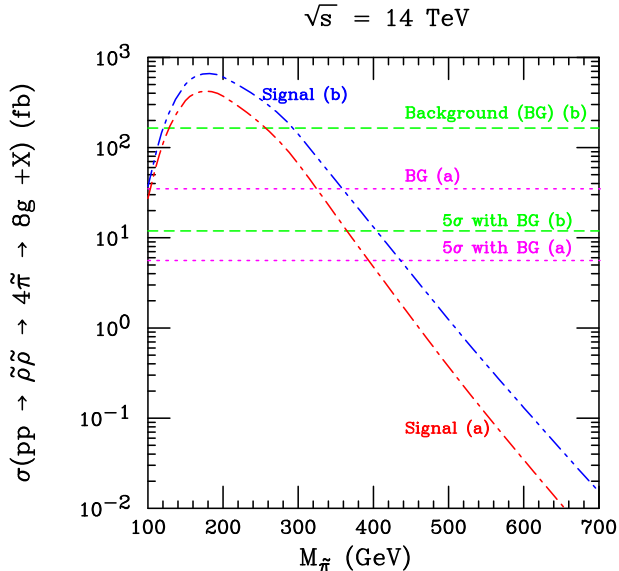

FIG. 14: The cross section for $pp \to \tilde{\rho}\tilde{\rho} \to 4\tilde{\pi} \to 8g + X$ as a function of $M_{\tilde{\pi}}$. We have applied all kinematic cuts and two sets of relative mass cuts: (a) $\Delta M_{2j} < 30$ GeV and $\Delta M_{4j} < 60$ GeV [red dot-dashed line], or (b) $\Delta M_{2j} < 50$ GeV and $\Delta M_{4j} < 100$ GeV [blue dot-dot-dashed line]. Also shown are the cross section for the dominant SM background with relative mass cut (a) [magenta dotted line] or (b) [green dashed line] as well as the minimal signal cross section that is required by a 5 sigma criterion with relative mass cut (a) [magenta (lower) dotted line] or (b) [green (lower) dashed line].

Fig. 14 shows the results for the *relative* mass window scheme with $(\Delta M_{ij} = 30\,\text{GeV}, \Delta M_{4j} = 60\,\text{GeV})$ and $(\Delta M_{ij} = 50\,\text{GeV}, \Delta M_{4j} = 100\,\text{GeV})$. We have used the ordered p_T cuts, $p_T(j_1, \ldots, j_8) > 320, 250, 200, 160, 125, 90, 60, 40$ GeV. These are the momentum cuts used for the low mass example in Ref. [6]. They are optimized for a $\tilde{\pi}$ mass around 225 GeV. With the cuts described above and an integrated luminosity of 30 fb^{-1} we can look for detection of hyper-pion masses out to 440 GeV ($M_{\tilde{\rho}} = 1460$ GeV) with the $\Delta M_{ij}/\Delta M_{4j} = 50/100$ GeV window or out to $M_{\tilde{\pi}} = 400$ GeV ($M_{\tilde{\rho}} = 1333$ GeV) with the 30/60 GeV windows.

Figs. 15 and 16 show our results for the *fixed* mass window scheme. We include two choices of p_T cuts and two mass window sizes as follows: (a)fixed mass windows with $\Delta M_{ij} = 0.10 M_{\tilde{\pi}}$ and $\Delta M_{4j} = 0.15 M_{\tilde{\rho}}$, or (b)fixed mass windows with $\Delta M_{ij} = 0.15 M_{\tilde{\pi}}$ and $\Delta M_{4j} = 0.20 M_{\tilde{\rho}}$. For Fig. 15 we apply the ordered p_T cuts as used above for the relative mass cuts, $p_T(j_1, \ldots, j_8) > 320, 250, 200, 160, 125, 90, 60, 40$ GeV. For Fig. 16 we use ordered cuts that scale as the hyper-pion mass for the four leading jets, $p_T(j_1, \ldots, j_4) > 1.5 M_{\tilde{\pi}}, 1.2 M_{\tilde{\pi}}, 1.0 M_{\tilde{\pi}}, 0.8 M_{\tilde{\pi}}$, and $p_T(j) > 50$ GeV for the four lowest p_T jets.
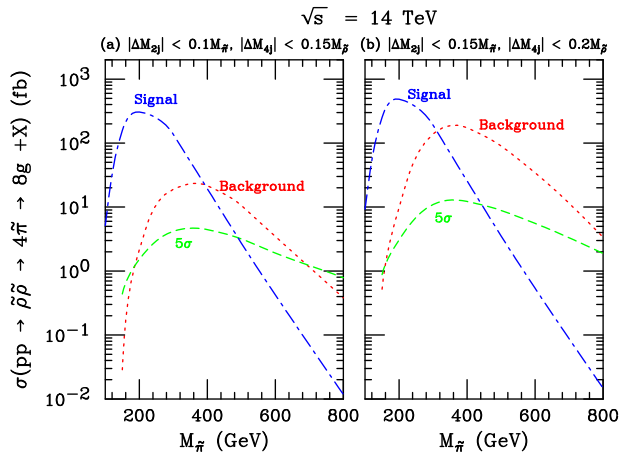

FIG. 15: The cross section for $pp \to \tilde{\rho}\tilde{\rho} \to 4\tilde{\pi} \to 8g + X$ (blue dot-dashed line) as a function of $M_{\tilde{\pi}}$ with acceptance cuts on p_T, η, and ΔR. We have applied two sets of fixed mass cuts: (a) $|M_{2j} - M_{\tilde{\pi}}| < 0.10 M_{\tilde{\pi}}$ and $|M_{4j} - M_{\tilde{\rho}}| < 0.15 M_{\tilde{\rho}}$, or (b) $|M_{2j} - M_{\tilde{\pi}}| < 0.15 M_{\tilde{\pi}}$ and $|M_{4j} - M_{\tilde{\rho}}| < 0.20 M_{\tilde{\rho}}$. The p_T cuts used were $p_T(j_1, \ldots, j_8) > 320, 250, 200, 160, 125, 90, 60, 40$ GeV. Also shown are the SM background cross section (σ_b)(red dotted line) and the minimal signal cross section that is required by a 5 sigma criterion (green dashed line) with an integrated luminosity of 30 fb^{-1}.

The scaled p_T cuts approximately capture the behaviour of the p_T distribution peaks for the leading jets in the model. At high masses the background could be further reduced by increasing the lower four p_T thresholds with relatively small reduction of the signal. However, above hyper-pion masses ~ 450 GeV both the signal and the background are too small to make detection of either likely with 30 fb^{-1} of integrated luminosity. At low masses these could be lowered to capture more of the signal without drastically enhancing the background. In general the p_T cuts could be tailored to reduce the background below signal for the entire mass range shown, but we do not want to be overly reliant on the model parameters we have chosen or to reduce the signal below practical detection limits. These cuts are a compromise
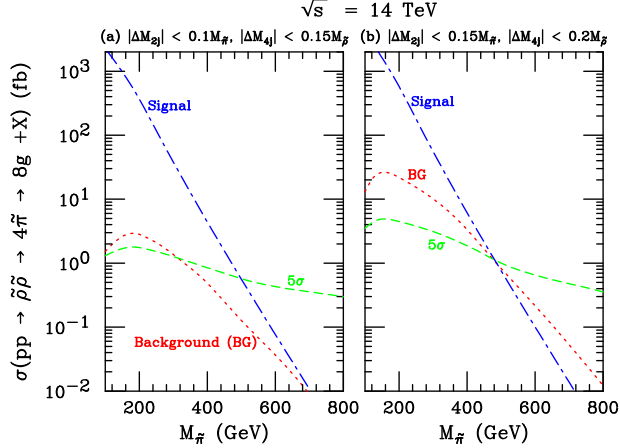
FIG. 16: The cross section for $pp \to \tilde{\rho}\tilde{\rho} \to 4\tilde{\pi} \to 8g + X$ (blue dot-dashed line) as a function of $M_{\tilde{\pi}}$ with acceptance cuts on p_T, η, and ΔR. We have applied two sets of fixed mass cuts: (a) $|M_{2j} - M_{\tilde{\pi}}| < 0.10 M_{\tilde{\pi}}$ and $|M_{4j} - M_{\tilde{\rho}}| < 0.15 M_{\tilde{\rho}}$, or (b) $|M_{2j} - M_{\tilde{\pi}}| < 0.15 M_{\tilde{\pi}}$ and $|M_{4j} - M_{\tilde{\rho}}| < 0.20 M_{\tilde{\rho}}$. This figure differs from Fig.15 in that the p_T cuts used here are $p_T(j_1) > 1.5 M_{\tilde{\pi}}$, $p_T(j_2) > 1.2 M_{\tilde{\pi}}$, $p_T(j_3) > M_{\tilde{\pi}}$, $p_T(j_4) > 0.8 M_{\tilde{\pi}}$, $p_T(j_5, j_6, j_7, j_8) > 50\,\text{GeV}$. Also shown are the SM background cross section (σ_b)(red dotted line) and the minimal signal cross section that is required by a 5 sigma criterion (green dashed line) with an integrated luminosity of $30\,\text{fb}^{-1}$.

to demonstrate the potential discrimination of signal from background due to the boost of massive decaying particles.

The fixed mass windows scale as the masses to capture the similarly scaling width of the coloron and the energy resolution of a real detector. Windows of $\Delta M_{ij} = 0.1 M_{\tilde{\pi}}$ and $\Delta M_{4j} = 0.15 M_{\tilde{\rho}}$ will require excellent resolution to be fully efficient. As in the relative window plots, we include a dashed line to estimate the discovery potential.

VII. SUMMARY AND CONCLUSIONS

Colorons, massive vector bosons in the color-octet representation, are a generic possibility for exotic physics which could be detected at the LHC. Both colorons and a set of scalar color-octet partners may emerge as the low energy phenomena of a generic new gauge group which becomes confining at high energy scales. This has the interesting consequence that relatively light colorons may evade dijet detection bounds by decaying first to a pair of

hyper-pions, each of which decays into a pair of gluons. Based on analogy with the chiral symmetry breaking interpretation of the Standard Model light mesons, the parameters of the theory can be determined in terms of a single unknown variable, $M_{\tilde{\rho}}$, at least for the case where the new hyper-color gauge group is $SU(3)$. Further, the phenomenology of the model should be fairly general even if we relax these assumptions.

We have implemented this model in the MadGraph framework and checked the resulting code against analytical computations, finding good agreement. Using this we have analyzed the signal $pp \to \tilde{\rho}\tilde{\rho} \to 4\tilde{\pi} \to 8g + X$ at the LHC. In this channel we can reconstruct both the coloron and hyper-pion resonances better than in the single coloron channel by using correlations between invariant masses.

We have simulated both the signal and background using two mass cut schemes, a relative window scheme which requires no foreknowledge of the relevant masses, and a fixed window scheme which demonstrates the power to discriminate against the background for specific choices of candidate masses. We find that with $30\,\mathrm{fb}^{-1}$ of integrated luminosity we can potentially detect such particles up to $M_{\tilde{\pi}} \simeq 495$ GeV and $M_{\tilde{\rho}} \simeq 1650$ GeV. For other integrated luminosities the reach in $M_{\tilde{\rho}}$, for one choice of cuts, is shown in Table I.

TABLE I: Discovery reach in the coloron mass, using the fixed mass cuts of Fig. 15(a), for several values of integrated luminosity.

Integrated Luminosity(fb^{-1}):	1	10	30	100	1000
Discovery Reach in $M_{\tilde{\rho}}$(GeV):	1250	1515	1650	1780	2080

In general, of course, we are sensitive to the choice of scales at tree level and a full predictive calculation would need to include effects of hadronization and jet reconstruction. Nonetheless, for a considerable range of parameters the signal can easily exceed the background even allowing for correction factors of order one. Our prospects improve significantly for increased jet energy resolution, leading to better reconstruction of invariant masses.

For the variety of related models with a similar phenomenology to the one we have considered, the fact that the hyper-mesons can be strongly produced once their mass thresholds are obtained, while avoiding the current dijet exclusion bounds, means they could be copiously produced at the LHC. As we gain experience with this collider, we have an excellent chance of discovering hyper-mesons or similar particles, if they exist, with masses up to

approximately 2 TeV.

[1] D. A. Dicus, C. D. McMullen and S. Nandi, Phys. Rev. D **65**, 076007 (2002) [arXiv:hep-ph/0012259].

[2] S. Cullen, M. Perelstein and M. E. Peskin, Phys. Rev. D **62**, 055012 (2000) [arXiv:hep-ph/0001166].

[3] C. T. Hill, Phys. Lett. B **266**, 419 (1991).

[4] D. A. Dicus, B. Dutta and S. Nandi, Phys. Rev. D **51**, 6085 (1995) [arXiv:hep-ph/9412370].

[5] C. Kilic, T. Okui and R. Sundrum, JHEP **0807**, 038 (2008) [arXiv:0802.2568 [hep-ph]].

[6] C. Kilic, S. Schumann and M. Son, JHEP **0904**, 128 (2009) [arXiv:0810.5542 [hep-ph]].

[7] C. Kilic, T. Okui, R. Sundrum, JHEP **1002**, 018 (2010). [arXiv:0906.0577 [hep-ph]].

[8] D. A. Dicus, C. Kao, S. Nandi and J. Sayre, Phys. Rev. D (2011) (to be published) [arXiv:1012.5694 [hep-ph]].

[9] T. Aaltonen *et al.* [CDF Collaboration], Phys. Rev. D **79**, 112002 (2009) [arXiv:0812.4036 [hep-ex]].

[10] V. Khachatryan *et al.* [CMS Collaboration], Phys. Rev. Lett. **105**, 211801 (2010) [arXiv:1010.0203 [hep-ex]].

[11] A. R. Zerwekh, Eur. Phys. J. **C70**, 917-920 (2010). [arXiv:1008.4575 [hep-ph]].

[12] B. A. Dobrescu, K. Kong and R. Mahbubani, Phys. Lett. B **670**, 119 (2008) [arXiv:0709.2378 [hep-ph]].

[13] T. Appelquist, H. C. Cheng and B. A. Dobrescu, Phys. Rev. D **64**, 035002 (2001) [arXiv:hep-ph/0012100].

[14] J. Pumplin, D. R. Stump, J. Huston, H. L. Lai, P. Nadolsky and W. K. Tung, JHEP **0207**, 012 (2002), [arXiv:hep-ph/0201195].

[15] T. Stelzer, W. F. Long, Comput. Phys. Commun. **81**, 357-371 (1994). [hep-ph/9401258].

[16] J. Alwall *et al.*, JHEP **0709**, 028 (2007) [arXiv:0706.2334 [hep-ph]].

[17] H. Murayama, I. Watanabe and K. Hagiwara, "HELAS: HELicity amplitude subroutines for Feynman diagram evaluations," KEK report KEK-91-11 (1992).

[18] ATLAS Collaboration, ATLAS Detector and Physics Performance Technical Design Report, CERN/LHCC 99-14/15 (1999); G. Aad *et al.* [The ATLAS Collaboration], "Expected Performance of the ATLAS Experiment - Detector, Trigger and Physics," arXiv:0901.0512 [hep-ex]

(2009).

[19] T. Gleisberg, S. Hoeche, F. Krauss, A. Schalicke, S. Schumann and J. C. Winter, JHEP **0402**, 056 (2004) [arXiv:hep-ph/0311263].

[20] T. Gleisberg and S. Hoeche, JHEP **0812**, 039 (2008) [arXiv:0808.3674 [hep-ph]].

[21] F. A. Berends and W. T. Giele, Nucl. Phys. B **306**, 759 (1988).

[22] C. Duhr, S. Hoeche and F. Maltoni, JHEP **0608**, 062 (2006) [arXiv:hep-ph/0607057].

[23] H. Baer, M. Bisset, C. Kao and X. Tata, Phys. Rev. D **46**, 1067 (1992).

[24] G. L. Bayatian *et al.* [CMS Collaboration], J. Phys. G **34**, 995 (2007).